Am J Nucl Med Mol Imaging 2024;14(1):41-47
www.ajnmmi.us /ISSN:2160-8407/ajnmmi0155449

*Original Article*

# Poly(ADP-ribose) polymerase (PARP)-targeted PET imaging in non-oncology application: a pilot study in preclinical models of nonalcoholic steatohepatitis

Troels E Jeppesen[1,3,4*], Tuo Shao[1,2*], Jiahui Chen[1,5], Jimmy S Patel[5,6], Xin Zhou[5], Andreas Kjaer[3,4], Steven H Liang[1,5]

*[1]Division of Nuclear Medicine, Department of Radiology, Harvard Medical School and Massachusetts General Hospital, Boston, MA, USA; [2]Division of Liver Center and Gastrointestinal, Department of Medicine, Massachusetts General Hospital, Boston, MA, USA; [3]Department of Clinical Physiology, Nuclear Medicine and PET and Cluster for Molecular Imaging, Copenhagen University Hospital - Rigshospitalet, Copenhagen, Denmark; [4]Department of Biomedical Sciences, University of Copenhagen, Copenhagen, Denmark; [5]Department of Radiology and Imaging Sciences, Emory University, Atlanta, GA, USA; [6]Department of Radiation Oncology, Winship Cancer Institute of Emory University, Atlanta, GA, USA. [*]Equal contributors.*

Received January 14, 2024; Accepted February 1, 2024; Epub February 20, 2024; Published February 28, 2024

**Abstract:** Poly(ADP-ribose) polymerase (PARP) activation often indicates a disruptive signal to lipid metabolism, the physiological alteration of which may be implicated in the development of non-alcoholic fatty liver disease. The objective of this study was to evaluate the capability of [$^{68}$Ga]DOTA-PARPi PET to detect hepatic PARP expression in a non-alcoholic steatohepatitis (NASH) mouse model. In this study, male C57BL/6 mice were subjected to a choline-deficient, L-amino acid-defined, high-fat diet (CDAHFD) for a 12-week period to establish preclinical NASH models. [$^{68}$Ga]DOTA-PARPi PET imaging of the liver was conducted at the 12-week mark after CDAHFD feeding. Comprehensive histopathological analysis, covering hepatic steatosis, inflammation, fibrosis, along with blood biochemistry, was performed in both NASH models and control groups. Despite the induction of severe inflammation, steatosis and fibrosis in the liver of mice with the CDAHFD-NASH model, PET imaging of NASH with [$^{68}$Ga]-DOTA-PARPi did not reveal a significantly higher uptake in NASH models compared to the control. This underscores the necessity for further development of new chelator-based PARP1 tracers with high binding affinity to enable the visualization of PARP1 changes in NASH pathology.

**Keywords:** Positron emission tomography (PET), poly(ADP-ribose) polymerase (PARP), non-alcoholic steatohepatitis, Gallium 68

## Introduction

Non-alcoholic steatohepatitis (NASH) represents an inflammatory subtype within the spectrum of non-alcoholic fatty liver disease. Although NASH can manifest without overt clinical symptoms, it can progress to cirrhosis over time, leading to significant morbidity and mortality. In the United States, the estimated lifetime direct medical costs for individuals with NASH reached $222 billion in 2017, with a projected increase due to the rising incidence of NASH cases [1]. Currently, the gold standard for diagnosing NASH is a liver biopsy, however, its utility is limited by its sensitivity and invasiveness [2]. In addition, non-invasive imaging techniques such as MRI and elastography, are limited in their ability to accurately diagnose fibrosis in patients with NASH. Although various biomarkers can offer some predictions of steatosis [3, 4], these alone do not possess the capability to consistently gauge the extent of the disease, therefore hindering the staging of steatosis and assessment of treatment response [2]. Thus, the development of novel non-invasive methods to accurately detect hepatic steatosis and fibrosis would hold significant clinical value.

Poly(ADP-ribose) polymerases (PARPs) are a family of enzymes with various functionality. One of their most significant functions is the ability to detect DNA damage with subsequent synthesis of ADP-ribose polymers which initiates the DNA repair cascade [5]. PARP inhibitors have demonstrated their clinical utility in the treatment of cancer [6, 7]. PARP1 plays a pivotal role not only in DNA repair but also in managing key cellular functions, including inflammation. NASH is marked by oxidative stress that results in the increased expression and activity of hepatic PARP [8]. Furthermore, studies indicate that inhibiting PARP or knocking out PARP1 or PARP2 genes can diminish liver damage, lower triglyceride levels in the liver, and reduce fibrosis and inflammation [9]. Additionally, recent efforts have led to the development of PARP-based positron emission tomography (PET) radioligands, such as [$^{18}$F]FluorThanatrace ([$^{18}$F]FTT) and [$^{18}$F]PARP-inhibitor ([$^{18}$F]PARPi), which have undergone first-in-human imaging studies for quantifying PARP expression levels in breast, ovarian, and head and neck cancer patients [10, 11]. Both of these radioligands derive from FDA approved PARP inhibitors. Development of PARP radioligands for assessment of pathologies beyond oncology continues to be an area of ongoing study [12]. With these advances, and the non-invasive yet robust quantitative imaging properties of PET, we postulated that a PARP-based PET radioligand may be able to detect PARP-induced inflammation

e-Century Publishing

**Table 1.** Radiochemical parameters for the [$^{68}$Ga]Ga-DOTA-PARPi (n=3)

| Peptide | RCY (%) | Molar Activity (mCi/μmol) | Activity (mCi) |
|---|---|---|---|
| [$^{68}$Ga]Ga-DOTA-PARPi | 70 ± 3 | 316 ± 53 | 3.1 ± 0.5 |

Molar activity calculated from starting peptide amount and end radioactivity.

in the setting of liver fibrosis and steatosis. In this study, we employed a well-established DOTA-PARPi tracer [13], to investigate its potential in imaging cellular death in NASH mouse models and determining the extent of PARP changes in the context of NASH.

## Materials and methods

*Animal models*

C57BL/6 mice were purchased from Charles River Laboratories (MA, USA). Mice were then fed the following diets for 14 weeks: standard chow (Prolab Isopro 3000; Scotts Distributing #8670) and CDAHFD (Research Diets A06071302; L-amino acid diet with 60 kcal% fat, 0.1% methionine, without added choline). All animals were housed in a pathogen-free, temperature-controlled animal facility with a 12-hour light-dark cycle. All protocols were reviewed and approved by the Institutional Animal Care and Use Committee of Massachusetts General Hospital.

*Radiochemistry*

$^{68}$Ga was obtained from a 20 mCi $^{68}$Ge/$^{68}$Ga generator (iThemba LAB, South Africa), and eluted with Ultrapure 0.6 M HCl (6 mL) in fractions of 0.5 mL each. The highest activity fraction was used without further processing. The DOTA-PARPi was synthesized as described previously [13]. All other chemicals were purchased from Sigma-Aldrich (St. Louis, MO) and used without further processing. Analytical HPLC was performed on a Shimadzu LC-10 VP system, with a single wavelength UV/VIS detector and a gradient of 5-95%, 0.1% TFA in MeCN/0.1% TFA in $H_2O$ over 10 minutes, with a Phenomenex kinetex 2.6 μm, C18, 50 × 4.6 mm column.

[$^{68}$Ga]Ga-DOTA-PARPi was synthesized as follows: 500 μL of 1 M NaOAc (pH 3.87) was added to 500 μL of $^{68}GaCl_3$ in 0.6 M HCl and the pH was adjusted to 4-4.5 by addition of 400 μL 1 M NaOH. DOTA-PARPi was added (2 mM, 5 μL, 10 nmol, in 1 M NaOAc), and the reaction mixture was incubated at 95°C for 10 min. The reaction was diluted with 10 mL of water, trapped onto a Waters C18 light column, and washed with 10 mL water. The radioactivity was eluted with 0.3 mL of EtOH, and the final product was formulated in PBS to under 5% EtOH. The product was confirmed by an analytical radio-HPLC.

*PET/CT*

CDAHFD and control mice were anesthetized with 1-2% isoflurane/air (v/v), and injected with [$^{68}$Ga]Ga-DOTA-PARPi (34-46 μCi, saline and <5% EtOH) via a tail vein catheter. Subsequent dynamic PET scanning over 60 minutes was performed on a G4 system (Sofie, VA) in a 3D list mode and the reconstruction of the dynamic PET images was performed using the manufacturer's software. Time-activity curves are presented as standardized uptake values.

*Histopathological analysis*

At the end of the feeding period, mice were weighed and euthanized. The livers were then carefully removed, weighed, and divided. Portions were promptly frozen in liquid nitrogen for subsequent protein and biochemical analyses, while others were preserved in 10% neutral-buffered formalin for histopathological examination. The liver tissue was further processed by embedding it in paraffin. Sections of 5 μm thickness were cut from the paraffin-embedded tissues and subjected to staining with H&E (Sigma, St. Louis, MO) or Sirius red F35B (Sigma, St. Louis, MO). Examination and analysis were performed using light microscopy.

*Western blot*

Protein samples were prepared using RIPA buffer with a protease inhibitor cocktail (Sigma, St. Louis, MO). Subsequently, the proteins were separated via SDS-PAGE and transferred onto a PVDF membrane. Primary antibodies employed included Rabbit anti-mouse PARP-1 (Cell Signaling Technology, Beverly, MA) and mouse anti-β-actin (Sigma, St. Louis, MO). For secondary antibodies, horseradish peroxidase (HRP)-conjugated enhanced chemiluminescence (ECL) donkey anti-rabbit IgG and HRP-conjugated ECL sheep anti-mouse IgG (GE Healthcare, Pittsburgh, PA) were used. The blots were then subjected to a chemiluminescence assay utilizing the Amersham ECL Western blotting detection kit (GE Healthcare, Pittsburgh, PA).

## Results

*Radiochemistry*

The DOTA-PARPi was radiolabeled with $^{68}$Ga in a one-step process with the radiochemical parameters detailed in **Table 1** and **Figure 1A**. A fractionated $^{68}$Ga elution from a $^{68}$Ge/$^{68}$Ga generator was employed. The resultant [$^{68}$Ga]Ga-DOTA-PARPi underwent analysis via analytical HPLC and was cross-validated by spiking with a standard, as depicted in **Figure 1B**, to confirm the identity of the product.

*In vitro evaluation of DOTA-PARPi and PARP1*

The inhibitory effect of DOTA-PARPi on PARP1 was determined by an $IC_{50}$ experiment, as illustrated in **Figure 1C**.

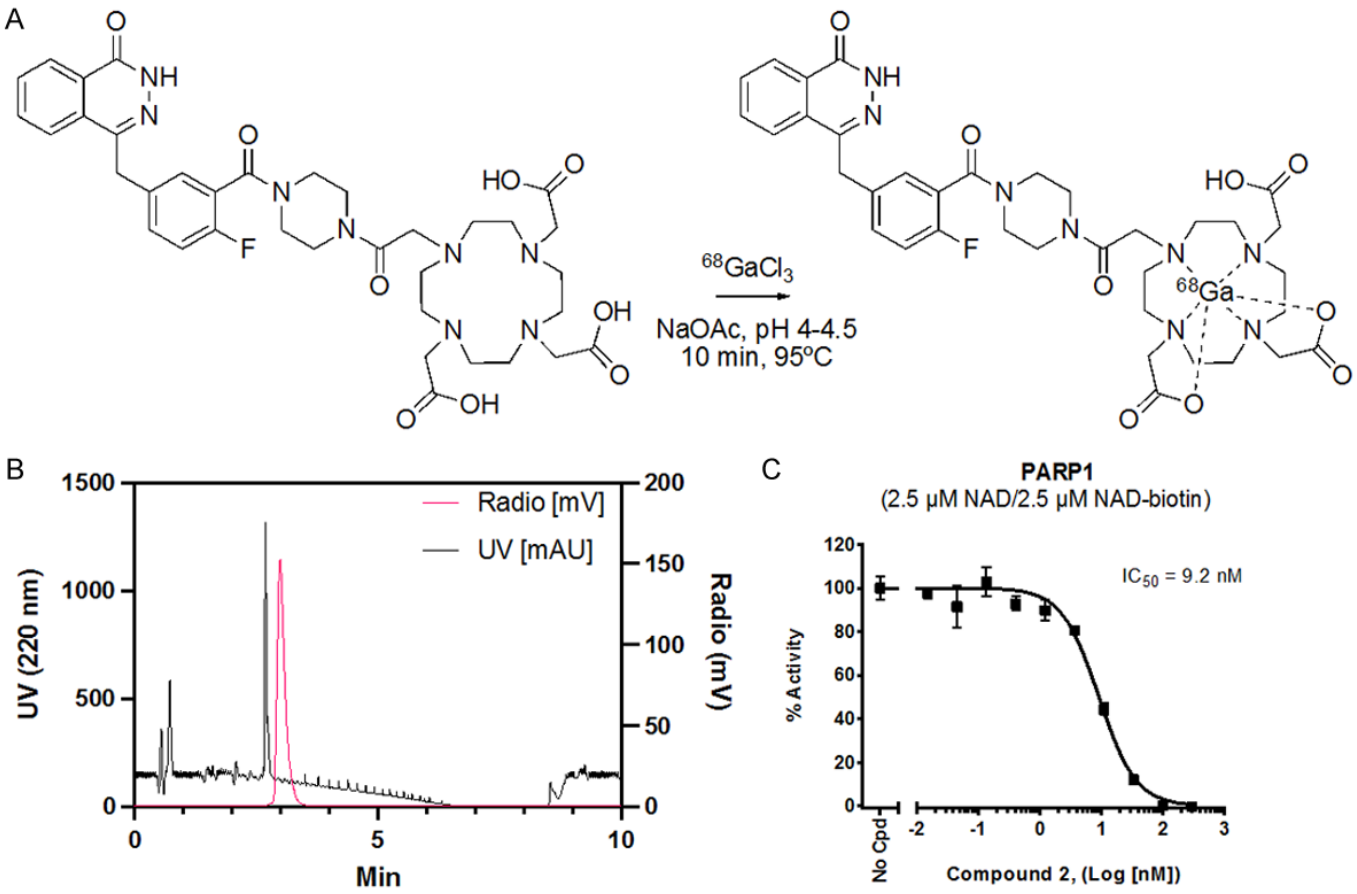


**Figure 1.** A. Conditions for labeling of DOTA-PARPi with $^{68}GaCl_3$. B. HPLC chromatogram of the spiked analytical sample. C. $IC_{50}$ determination of DOTA-PARPi towards PARP1, evaluated from $NAD^+$ activity.

In the experiment, PARP1 was subjected to a 2.5 μM NAD/2.5 μM NAD-biotin mixture, and its activity was measured against increasing concentrations of DOTA-PARPi. Activity was quantified using a PARP1 chemiluminescence assay kit (BPS number 80551) and olaparib as a positive control ($IC_{50}$=0.51 nM). The $IC_{50}$ of DOTA-PARPi was determined to be 9.2 nM, indicating its potency on PARP1 activity (**Figure 1C**).

*Liver histopathology in CDAHFD-fed mice*

Validation of the mouse NASH models was carried out through histology staining. Hematoxylin and eosin (H&E) staining revealed evident steatosis, distinct hepatocyte ballooning, and lobular inflammation, as illustrated in **Figure 2A**. Fibrosis was further confirmed using Sirius red staining, where collagen fibers are depicted in red. The extent of fibrosis observed was severe, indicating the presence of clear NASH with fibrosis in the model (**Figure 2B**).

*Hepatic expression of PARP1 in CDAHFD-fed mice*

The alteration in PARP1 levels in NASH liver tissue was assessed through western blotting of homogenized liver tissue from NASH mice and control mice, as depicted in **Figure 3**. β-actin served as the housekeeping gene, and the expression of PARP1 in both control and NASH models was normalized to β-actin. The results demonstrated a significant 5.2-fold increase in PARP1 expression in the NASH model compared to the control group (P<0.01).

*In vivo imaging*

In vivo imaging was conducted on NASH mouse models subjected to a CDAHFD diet. Age-matched mice on a regular diet were employed as control groups. The imaging protocol involved the injection of [$^{68}$Ga]Ga-DOTA-PARPi, followed by a dynamic PET scan spanning 60 minutes. The PET data, as illustrated in **Figure 4**, revealed that the area under the curve (AUC) does not exhibit significant differences compared to the AUC of control mice. This observation suggests that [$^{68}$Ga]Ga-DOTA-PARPi is not suitable for monitoring PARP changes in the CDAHFD NASH models.

## Discussion

PARP enzymes, recognized for their critical role in DNA repair mechanisms, have been implicated in additional biological processes beyond cancers, such as managing oxidative stress, maintaining mitochondrial functionality, and regulating intermediary metabolism [14, 15]. These processes are notably implicated in the pathogenesis of

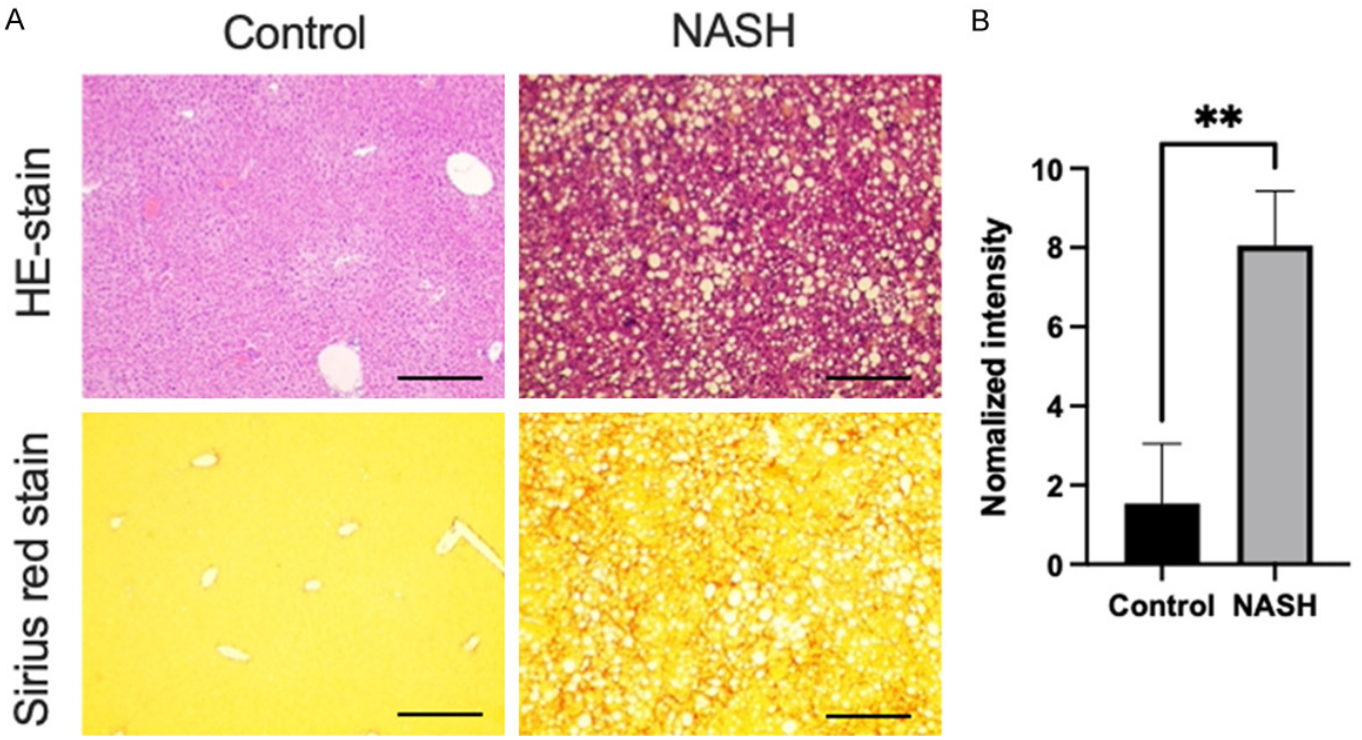


**Figure 2.** A. HE and Sirius Red staining of control mice liver tissue and NASH mice liver tissue (Scale bar 200 μm, original magnification ×20). B. Normalized Sirius Red intensity obtained from A. Data are presented as the mean ± standard error of the mean. **P<0.01 compared with the control group.

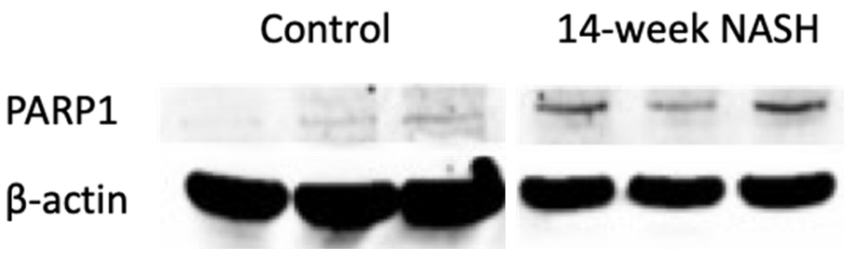


**Figure 3.** Protein level of PARP1 in the livers of control and choline-deficient, L-amino acid-defined, high-fat diet (CDAHFD)-fed mice.

NASH [9, 16]. Earlier findings have highlighted the induction of PARP in cirrhotic conditions and the therapeutic benefits of PARP inhibition in liver fibrosis models. By employing a NASH mouse model, induced either by a high-fat diet or by diets lacking methionine and choline, previous studies have demonstrated that a high-fat diet correlated with increased PARP1 expression [17]. In contrast, treatment with PARP inhibitors was observed to mitigate liver damage, steatosis, metabolic imbalances, and inflammatory and fibrotic responses in these models. With overexpression of PARP in these physiological conditions, we hypothesized that a novel PARP PET tracer would be a useful molecular imaging tool in monitoring cellular death in the progression of NASH.

PET is a widely used physiological imaging technique employed in healthcare for diagnostic purposes. The most prevalent radiotracers for PET imaging are those that are utilized for tissue metabolism such as [$^{18}$F]fluorodeoxyglucose ([$^{18}$F]FDG). However, these tracers tend to be non-specific to the disease processes in question and may be masked by physiological uptake by surrounding tissue. The development of PET tracers that bind to markers specific of a disease process is an area that is currently under investigation. In the context of the well-established role of PARP1 as a mediator of liver inflammation [18], a PET tracer specifically targeting PARP aligns seamlessly with this thematic focus. One of the most prominent PARP specific radiotracers includes [$^{18}$F]FTT which has been studied in a variety of oncologic models and is currently under early phase clinical investigation [19-21]. Additionally, there are several PARP based radiotracers that derive their structure from FDA-approved PARP inhibitors and are currently under investigation as diagnostic tools in various disease sites. As an example, [$^{18}$F]FTT derives its structure from rucaparib, and had preclinical validation as well as early phase I/II evaluation for patients with breast and ovarian cancer. Radiolabeled Olaparib has been studied in ovarian cancer, glioblastoma, and pancreatic cancer [22-24]. In a similar vein, $^{18}$F-PARPi, which derives from Olaparib, has been studied in various clinical models [11, 25]. In contrast to well-established small molecule PARP PET ligands with validated imaging efficacy in both preclinical and clinical studies, we selected a chelator-based [$^{68}$Ga]Ga-DOTA-PARPi for our investigation for the following reasons. Our

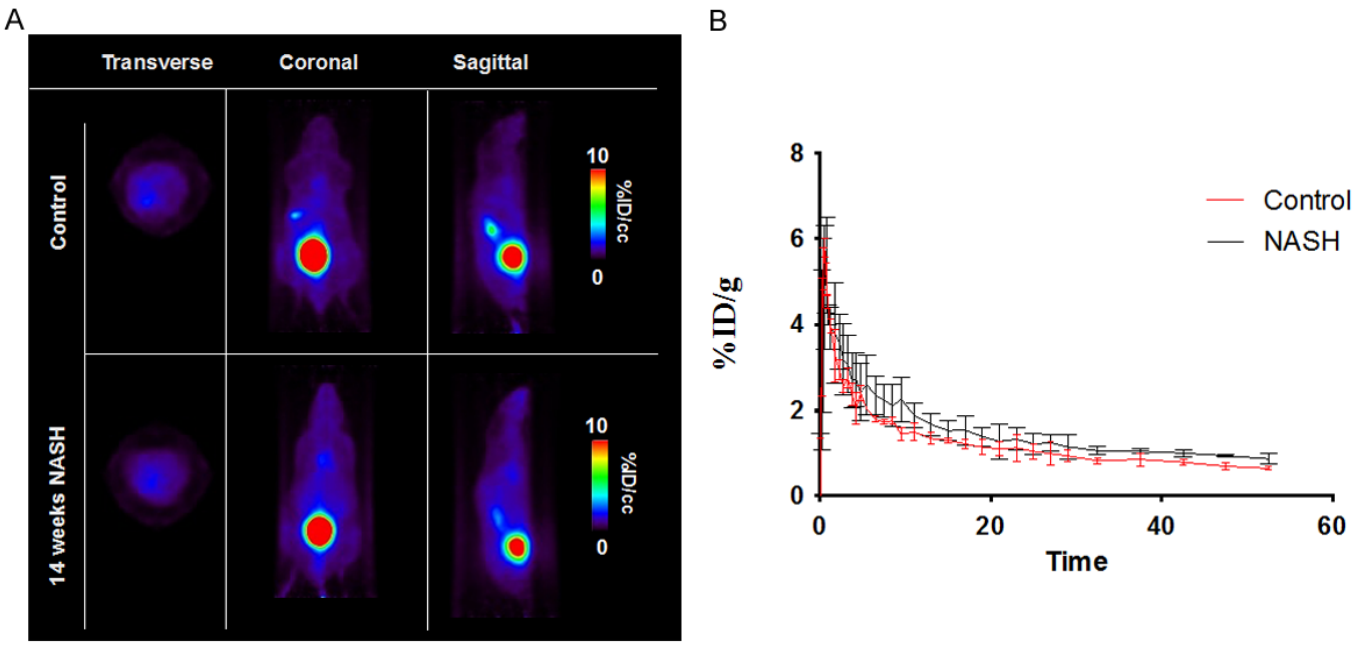


**Figure 4.** PET acquisition data for [$^{68}$Ga]Ga-DOTA-PARPi. A. Representative images from PET. Images are transverse, dorsal and side-views going from left to right. B. Quantification of the PET data over time. n=2 pr. Group.

primary objective is to detect changes in PARP1 expression and distribution in a preclinical model of NASH. The prevalent issue with most small molecule based PARP tracers lies in their tendency to exhibit high background activity in primary metabolic organs, such as the liver, small intestine, and kidneys - common routes of elimination in the body. This poses a potential confounding factor when attempting to distinguish subtle radioactive signal changes, particularly with our focal area of interest, the liver. To address this concern, we intentionally selected a chelator-based PARP ligand, specifically [$^{68}$Ga]Ga-DOTA-PARPi. This choice is underpinned by its favorable renal clearance and resulting low non-specific imaging background in the liver. These inherent characteristics would enable us to precisely identify subtle uptake changes through PET imaging in our preclinical models. Furthermore, due to the exploratory nature of our work, a validated tracer, such as DOTA-PARPi validated in oncology models, could be easily adopted in our study without modifying other molecular properties. DOTA-PARPi exhibited a favorable inhibitory concentration of 9.2 nM, rendering it suited for utilization as a radioactive tracer in our pilot study.

The synthesis of the tracer [$^{68}$Ga]Ga-DOTA-PARPi was achieved with high yield, enabling our subsequent imaging studies. In vivo imaging utilizing [$^{68}$Ga]Ga-DOTA-PARPi was conducted to assess its potential as a molecular imaging tool for non-alcoholic steatohepatitis (NASH). This study included two cohorts: one comprising mice on a choline-deficient, L-amino acid-defined, high-fat diet (CDAHFD), which induces NASH, and a control group of mice on a standard diet. Both groups were age-matched to ensure consistency in developmental factors that could influence PET imaging results. Validation of the NASH model was conducted through HE and Sirius red staining of histology slides, revealing evident fibrosis in NASH mice and its absence in the control group. It is worth highlighting that PARP1 expression was significantly upregulated (greater than five-fold) in the NASH model compared to the control, confirmed by Western blotting analysis. These results provided the biological evidence and reflected the substantial PARP1 expression level difference in the fibrosis models.

The dynamic PET scans were performed over a span of 60 minutes post-injection of the tracer. From PET imaging results, we observed favorable low background uptake in the normal liver tissues and relatively high bladder uptake, which indicated rapid washout of the radiotracer primarily through renal clearance. This advantageous clearance profile may help reduce non-specific background uptake in the liver during the NAFLD. The quantitative analysis of the PET imaging, as illustrated in **Figure 4**, reveals that the tracer uptake, expressed as the area under the time-activity curve (AUC), shows no significant distinction between the NASH-induced mice and the controls. This is an unexpected result, as tracers in PET imaging are typically anticipated to display differential uptake in diseased versus normal tissues. The lack of significant AUC difference implies that [$^{68}$Ga]Ga-DOTA-PARPi does not have the specificity required to act as an effective imaging biomarker for NASH in this context. For a more comprehensive interpretation, it would be beneficial to compare these findings with reported tracers known for their effectiveness in NASH imaging. For example, tracers that target ([$^{18}$F]Alfatide, targeting integrin $\alpha_v\beta_3$) specific fibrosis

pathways or inflammation associated with NASH could provide a contrasting reference point [26]. It is notable that [$^{18}$F]Alfatide showed increased uptake in diseased liver tissue due to the altered fibrosis or inflammation characteristic of NASH.

To guide future studies, pharmacological and physiochemical properties of [$^{68}$Ga]Ga-DOTA-PARPi relative to successful NASH tracers have been analyzed to provide insights into the design of more effective PET probes for imaging NASH. In general, small molecule based PARP tracers demonstrated superior binding affinity and/or potency to chelator based counterparts. Imaging of NASH with [$^{68}$Ga]Ga-DOTA-PARPi did not exhibit a significantly higher uptake in the NASH model compared to the control, potentially due to low binding affinity to PARP1 *in vivo*. Additional factors such as lipophilicity and metabolic stability are also key differentiators that could influence tracer uptake and retention in NASH-affected tissue. Subsequent medicinal chemistry optimization is imperative to enhance the ligand sensitivity of next generation [$^{68}$Ga]Ga-DOTA-PARPi PET probes while maintaining its elimination pathway, to monitor PARP1 changes in the liver.

## Conclusion

In summary, DOTA-PARPi demonstrated satisfactory binding to PARP1 and was successfully radiolabeled with $^{68}$Ga in a straightforward process with high yield. Although our biological hypothesis, validated by Western blotting, confirmed the upregulation of PARP1 in the NASH disease model mice, the tracer [$^{68}$Ga]Ga-DOTA-PARPi did not detect significant changes in liver uptake and retention. Ongoing medicinal chemistry efforts aim to enhance binding affinity while maintaining the chelator-based tracer design, contributing to a favorable renal clearance profile and low non-specific background uptake in the liver.

## Acknowledgements

TEJ was supported by grants from Fulbright Denmark, The Lundbeck Foundation, Eva and Henry Frænkels foundation, The Danish Cancer Society, The Harboe Foundation, Dr. phil Ragna Rask-Nielsens Grundforskningsfond, Kong Christian den Tiendes fond, Carl og Ellen Hertz' legat, The Scandinavian Society of Clinical Physiology and Nuclear Medicine, Christian og Otilla Brorsons Rejselegat, A.P. Møller fonden and Helsefonden. JSP is supported by NCI T32CA275777.

## Disclosure of conflict of interest

None.

**Address correspondence to:** Steven H Liang, Department of Radiology and Imaging Sciences, Emory University, Atlanta, GA, USA. E-mail: Steven.liang@emory.edu

## References

[1] Sheka AC, Adeyi O, Thompson J, Hameed B, Crawford PA and Ikramuddin S. Nonalcoholic steatohepatitis: a review. JAMA 2020; 323: 1175-1183.

[2] Piazzolla VA and Mangia A. Noninvasive diagnosis of NAFLD and NASH. Cells 2020; 9: 1005.

[3] Sripongpun P, Kim WR, Mannalithara A, Charu V, Vidovszky A, Asch S, Desai M, Kim SH and Kwong AJ. The steatosis-associated fibrosis estimator (SAFE) score: a tool to detect low-risk NAFLD in primary care. Hepatology 2023; 77: 256-267.

[4] Dowman JK, Tomlinson JW and Newsome PN. Systematic review: the diagnosis and staging of non-alcoholic fatty liver disease and non-alcoholic steatohepatitis. Aliment Pharmacol Ther 2011; 33: 525-540.

[5] Ryu KW, Kim DS and Kraus WL. New facets in the regulation of gene expression by ADP-ribosylation and poly(ADP-ribose) polymerases. Chem Rev 2015; 115: 2453-2481.

[6] Underhill C, Toulmonde M and Bonnefoi H. A review of PARP inhibitors: from bench to bedside. Ann Oncol 2011; 22: 268-279.

[7] Mateo J, Lord CJ, Serra V, Tutt A, Balmaña J, Castroviejo-Bermejo M, Cruz C, Oaknin A, Kaye SB and de Bono JS. A decade of clinical development of PARP inhibitors in perspective. Ann Oncol 2019; 30: 1437-1447.

[8] Ray K. Steatohepatitis: PARP inhibition protective against alcoholic steatohepatitis and NASH. Nat Rev Gastroenterol Hepatol 2017; 14: 3.

[9] Mukhopadhyay P, Horváth B, Rajesh M, Varga ZV, Gariani K, Ryu D, Cao Z, Holovac E, Park O, Zhou Z, Xu MJ, Wang W, Godlewski G, Paloczi J, Nemeth BT, Persidsky Y, Liaudet L, Haskó G, Bai P, Boulares AH, Auwerx J, Gao B and Pacher P. PARP inhibition protects against alcoholic and non-alcoholic steatohepatitis. J Hepatol 2017; 66: 589-600.

[10] Lee HS, Schwarz SW, Schubert EK, Chen DL, Doot RK, Makvandi M, Lin LL, McDonald ES, Mankoff DA and Mach RH. The development of (18)F fluorthanatrace: a PET radiotracer for imaging poly (ADP-Ribose) polymerase-1. Radiol Imaging Cancer 2022; 4: e210070.

[11] Schöder H, França PDS, Nakajima R, Burnazi E, Roberts S, Brand C, Grkovski M, Mauguen A, Dunphy MP, Ghossein RA, Lyashchenko SK, Lewis JS, O'Donoghue JA, Ganly I, Patel SG, Lee NY and Reiner T. Safety and feasibility of PARP1/2 imaging with (18)F-PARPi in patients with head and neck cancer. Clin Cancer Res 2020; 26: 3110-3116.

[12] Tong J, Chen B, Tan PW, Kurpiewski S and Cai Z. Poly (ADP-ribose) polymerases as PET imaging targets for central nervous system diseases. Front Med (Lausanne) 2022; 9: 1062432.

[13] Huang T, Hu P, Banizs AB and He J. Initial evaluation of Cu-64 labeled PARPi-DOTA PET imaging in mice with mesothelioma. Bioorg Med Chem Lett 2017; 27: 3472-3476.

[14] de la Lastra CA, Villegas I and Sánchez-Fidalgo S. Poly(ADP-ribose) polymerase inhibitors: new pharmacological functions and potential clinical implications. Curr Pharm Des 2007; 13: 933-962.

[15] Tapodi A, Debreceni B, Hanto K, Bognar Z, Wittmann I, Gallyas F Jr, Varbiro G and Sumegi B. Pivotal role of Akt activation in mitochondrial protection and cell survival by poly(ADP-ribose)polymerase-1 inhibition in oxidative stress. J Biol Chem 2005; 280: 35767-35775.

[16] Gariani K, Ryu D, Menzies KJ, Yi HS, Stein S, Zhang H, Perino A, Lemos V, Katsyuba E, Jha P, Vijgen S, Rubbia-Brandt L, Kim YK, Kim JT, Kim KS, Shong M, Schoonjans K and Auwerx J. Inhibiting poly ADP-ribosylation increases fatty acid oxidation and protects against fatty liver disease. J Hepatol 2017; 66: 132-141.

[17] Huang K, Du M, Tan X, Yang L, Li X, Jiang Y, Wang C, Zhang F, Zhu F, Cheng M, Yang Q, Yu L, Wang L, Huang D and Huang K. PARP1-mediated PPARα poly(ADP-ribosyl)ation suppresses fatty acid oxidation in non-alcoholic fatty liver disease. J Hepatol 2017; 66: 962-977.

[18] Mukhopadhyay P, Rajesh M, Cao Z, Horváth B, Park O, Wang H, Erdelyi K, Holovac E, Wang Y, Liaudet L, Hamdaoui N, Lafdil F, Haskó G, Szabo C, Boulares AH, Gao B and Pacher P. Poly (ADP-ribose) polymerase-1 is a key mediator of liver inflammation and fibrosis. Hepatology 2014; 59: 1998-2009.

[19] Zhou D, Chu W, Xu J, Jones LA, Peng X, Li S, Chen DL and Mach RH. Synthesis, [$^{18}$F] radiolabeling, and evaluation of poly (ADP-ribose) polymerase-1 (PARP-1) inhibitors for in vivo imaging of PARP-1 using positron emission tomography. Bioorg Med Chem 2014; 22: 1700-1707.

[20] Makvandi M, Pantel A, Schwartz L, Schubert E, Xu K, Hsieh CJ, Hou C, Kim H, Weng CC, Winters H, Doot R, Farwell MD, Pryma DA, Greenberg RA, Mankoff DA, Simpkins F, Mach RH and Lin LL. A PET imaging agent for evaluating PARP-1 expression in ovarian cancer. J Clin Invest 2018; 128: 2116-2126.

[21] Puentes LN, Makvandi M and Mach RH. Molecular imaging: PARP-1 and beyond. J Nucl Med 2021; 62: 765-770.

[22] Wang X, Liu W, Li K, Chen K, He S, Zhang J, Gu B, Xu X and Song S. PET imaging of PARP expression using (68)Ga-labelled inhibitors. Eur J Nucl Med Mol Imaging 2023; 50: 2606-2620.

[23] Chan CY, Hopkins SL, Guibbal F, Pacelli A, Baguña Torres J, Mosley M, Lau D, Isenegger P, Chen Z, Wilson TC, Dias G, Hueting R, Gouverneur V and Cornelissen B. Correlation between molar activity, injection mass and uptake of the PARP targeting radiotracer [(18)F]olaparib in mouse models of glioma. EJNMMI Res 2022; 12: 67.

[24] Wilson TC, Xavier MA, Knight J, Verhoog S, Torres JB, Mosley M, Hopkins SL, Wallington S, Allen PD, Kersemans V, Hueting R, Smart S, Gouverneur V and Cornelissen B. PET imaging of PARP expression using (18)F-olaparib. J Nucl Med 2019; 60: 504-510.

[25] Ambur Sankaranarayanan R, Kossatz S, Weber W, Beheshti M, Morgenroth A and Mottaghy FM. Advancements in PARP1 targeted nuclear imaging and theranostic probes. J Clin Med 2020; 9: 2130.

[26] Shao T, Chen Z, Belov V, Wang X, Rwema SH, Kumar V, Fu H, Deng X, Rong J, Yu Q, Lang L, Lin W, Josephson L, Samir AE, Chen X, Chung RT and Liang SH. [(18)F]-Alfatide PET imaging of integrin αvβ3 for the non-invasive quantification of liver fibrosis. J Hepatol 2020; 73: 161-169.